Consideration of soil types for the calibration of molecular proxies for soil pH and temperature using global soil datasets and Vietnamese soil profiles

Nina Davtian, Guillemette Ménot, Edouard Bard, Jérôme Poulenard, Pascal Podwojewski

Consideration of soil types for the calibration of molecular proxies for soil pH and temperature using global soil datasets and Vietnamese soil profiles

Nina Davtian [a,*], Guillemette Ménot [b], Edouard Bard [a], Jérôme Poulenard [c], Pascal Podwojewski [d,e]

[a] *Aix-Marseille Université, CNRS, IRD, Collège de France, CEREGE UM34, Aix-en-Provence 13545, France*

[b] *Laboratoire de Géologie de Lyon, Terre, Planètes, Environnement, CNRS UMR 5276, Ecole Normale Supérieure de Lyon, Université Claude Bernard Lyon 1, France*

[c] *EDYTEM, Université de Savoie/CNRS, 73376 Le Bourget du Lac, France*

[d] *IRD, UMR 242 IEES-Paris, 32 avenue Henri Varagnat, 93143 Bondy cedex, France*

[e] *IRD, UMR 242 IEES-Paris, School of Agriculture, Earth and Environmental Science, University of KwaZulu-Natal, Box X01, Scottsville, 3209, South Africa*

*Corresponding author. *E-mail address*: davtian@cerege.fr (N. Davtian)

21

ABSTRACT

Distribution of branched glycerol dialkyl glycerol tetraethers (brGDGTs) in soils depends on environmental parameters such as mean annual air temperature (MAAT) and soil pH. MBT′/MBT′$_{5ME}$ (methylation index of branched tetraethers) and CBT/CBT′ (cyclization ratio of branched tetraethers) are ratios based on the relative abundances of brGDGTs. Using these ratios, global and regional/local calibrations have been established using surface soils, but generally without any preliminary study of soil types. In this study, we reconsider global MAAT–pH/brGDGT calibrations by assigning soil types to the 358 components of a composite soil dataset. Additionally, we investigate brGDGT-derived proxies in five well-described soil profiles along an altitudinal transect in the Mount Fan Si Pan National Park, northwestern Vietnam. Our results show that at the global scale, traditional MAAT–pH/brGDGT relationships per soil type are significantly different and that MAAT(pH) residuals per soil type may differ as well, for example between Alisols and Podzols. This effect persists when 5- and 6-methyl brGDGTs are quantified separately. In addition, MAAT(pH) residuals per soil type are generally not clearly reduced, including in Leptosols, in which 6-methyl brGDGTs are present. In the Fan Si Pan transect, MBT′/CBT–MAAT estimates showed no significant deviation from expected MAATs. We find, however, that soil type effect – related to vegetation changes and contrasting soil organic carbon properties – may bias MAAT–pH estimates in the Vietnamese soil transect. Additionally, soil

depth plays a role which differs between the different Fan Si Pan soil profiles, likely determined by soil type and history.

Keywords: calibration, soil, brGDGTs, temperature, pH

1. Introduction

Branched glycerol dialkyl glycerol tetraethers (brGDGTs) are membrane lipids of high molecular weight (Fig. 1) that are of bacterial origin (Weijers et al., 2006a, 2009; Sinninghe Damsté et al., 2011, 2014). They are ubiquitous in aquatic and continental environments (Schouten et al., 2013 and references therein). At the global scale, brGDGT distributions in soils mainly depend on mean annual air temperature (MAAT) and soil pH (e.g., Weijers et al., 2007; Peterse et al., 2012). Several indices have been developed to summarize brGDGT distributions, for instance the methylation index of branched tetraethers (MBT), the cyclization ratio of branched tetraethers (CBT) and the MBT′ index, which is a simplified form of MBT. These indices are linked to continental temperatures and soil pH through two global soil calibrations. However, calibration errors are about 5.0 °C and about 0.8 pH unit (Weijers et al., 2007; Peterse et al., 2012). High calibration errors are due to multiple possible biases such as soil texture, humidity and oxygenation (e.g. Peterse et al., 2009a; Huguet et al., 2010; Dirghangi et al., 2013; Menges et al., 2014; Dang et al., 2016), seasonality and/or use of atmospheric rather than soil temperature (e.g., Peterse et al., 2012; Deng et al., 2016; Wang et al., 2016). Indeed, MAAT is an approximation of mean annual soil temperature that is also influenced by other climate-dependent parameters, such as snow cover, vegetation type and soil properties (Smerdon et al., 2004). Recently, new indices such as MBT'_{5ME}, CBT_{5ME} and CBT′ have been defined, following analytical

improvements that have allowed the separate quantification of 5- and 6-methyl brGDGTs (Fig. 1; De Jonge et al., 2014). Poor brGDGT separations also explain part of the scatter in the global calibrations (De Jonge et al., 2014).

As also seen at the global scale, substantial scatter has been observed at the regional/local scale, including for calibrations based on altitudinal transects (Sinninghe Damsté et al., 2008; Peterse et al., 2009b; Yang et al., 2010, 2015b; Ernst et al., 2013; Liu et al., 2013; Anderson et al., 2014; Coffinet et al., 2014; Zhuang et al., 2015; Deng et al., 2016; Nieto-Moreno et al., 2016). Factors other than MAAT and pH, such as vegetation and soil type, length of growing season and topography, have been suggested as causes for part of the scatter (Sinninghe Damsté et al., 2008; Peterse et al., 2009b; Liu et al., 2013; Anderson et al., 2014; Deng et al., 2016; Nieto-Moreno et al., 2016). Contrary to the classical MBT′ index, MBT'_{5ME} is well correlated with MAAT/altitude at Mt. Shennongjia, China (Yang et al., 2015a, 2015b). It is noteworthy that only a few previous brGDGT-based studies have used well-described soils and/or profiles (Huguet et al., 2010; Zech et al., 2012; Menges et al., 2014; Yamamoto et al., 2016). A better consideration of soil pedogenesis may help researchers to properly evaluate the dependency of the observed scatters on soil physico-chemical properties.

In the present study, we reassess a composite global soil dataset (Huguet et al., 2010; Peterse et al., 2012; Dirghangi et al., 2013; Anderson et al., 2014; De Jonge et al., 2014) by assigning a soil type to each of its 358

components to investigate traditional and newest MAAT–pH/brGDGT relationships as well as MAAT(pH) residuals, per soil type. We also take advantage of a well-characterized altitudinal soil transect with an elevation range of 1400 m in the Mount Fan Si Pan National Park, Vietnam (Podwojewski et al., 2011) to investigate brGDGT distributions. We focus, in particular, on the possible vegetation/soil type and depth effect and assess how well brGDGT-derived proxies reflect MAAT and soil pH in Vietnam.

2. Materials and methods

2.1. Soil type assignment for the global soil dataset and statistical analysis

A composite global soil dataset of 358 previously analyzed samples (Supplementary Table S1; Huguet et al., 2010; Peterse et al., 2012; Dirghangi et al., 2013; Anderson et al., 2014; De Jonge et al., 2014) was used for soil type assignment. For most samples taken from the International Soil Reference and Information Centre (ISRIC), soil types were obtained using the ISRIC Soil Information System (ISIS) database (http://isis.isric.nl, last accessed on Thursday, August 25, 2016). For the other samples, with the exception of those analyzed by Huguet et al. (2010) which were the subject of preliminary pedological studies, the most likely soil type was selected using the SoilInfo App based on SoilGrids1km (Hengl et al., 2014; https://soilinfo-app.org, version 0.5.0, 15 November, 2015, accessed before the update to SoilGrids250m in June 2016).

Statistical analysis – correlation tests, linear regressions and homogeneity of slopes test/analysis of covariance (ANCOVA) – was conducted using the statistical software R 3.1.2 (R Development Core Team, 2016). Prior to the investigation of each MAAT–brGDGT and each pH–brGDGT relationship, the outliers were eliminated using the car package (Fox and Weisberg, 2011). After conducting repeated outlier tests until no more samples with a Bonferroni p-value < 0.05 remained, all the identified outliers were excluded from further statistical analysis. The slope homogeneity test was then conducted to verify whether regression slopes per soil type for a given MAAT–brGDGT or pH–brGDGT relationship were statistically identical – the ANCOVA being conducted only when the homogeneity of slopes test was not significant, i.e. p-value ≥ 0.05. Only soil types with at least 10 samples after exclusion of outliers and samples with missing data were selected for statistical analysis.

All MAAT–pH residuals in this study were determined using the global soil calibrations of Peterse et al. (2012) following equations (1) and (2), and of De Jonge et al. (2014) following equations (3) and (4):

$$\mathrm{MAAT} = 0.81 - 5.67 \times \mathrm{CBT} + 31.00 \times \mathrm{MBT'} \quad (1)$$

$$\mathrm{pH} = 7.90 - 1.97 \times \mathrm{CBT} \quad (2)$$

$$\mathrm{MAAT} = -8.57 + 31.45 \times \mathrm{MBT'_{5ME}} \quad (3)$$

$$\mathrm{pH} = 7.15 + 1.59 \times \mathrm{CBT'} \quad (4)$$

With MBT′, CBT, $\mathrm{MBT'_{5ME}}$ and CBT′ defined as follows:

$$\mathrm{MBT'} = \frac{\mathrm{Ia} + \mathrm{Ib} + \mathrm{Ic}}{\mathrm{Ia} + \mathrm{Ib} + \mathrm{Ic} + \mathrm{IIa} + \mathrm{IIb} + \mathrm{IIc} + \mathrm{IIIa} + \mathrm{IIa'} + \mathrm{IIb'} + \mathrm{IIc'} + \mathrm{IIIa'}} \quad (5)$$

$$\mathrm{CBT} = -\log\left(\frac{\mathrm{Ib} + \mathrm{IIb} + \mathrm{IIb'}}{\mathrm{Ia} + \mathrm{IIa} + \mathrm{IIa'}}\right) \quad (6)$$

$$\mathrm{MBT'_{5ME}} = \frac{\mathrm{Ia} + \mathrm{Ib} + \mathrm{Ic}}{\mathrm{Ia} + \mathrm{Ib} + \mathrm{Ic} + \mathrm{IIa} + \mathrm{IIb} + \mathrm{IIc} + \mathrm{IIIa}} \quad (7)$$

$$\mathrm{CBT'} = \log\left(\frac{\mathrm{Ic} + \mathrm{IIa'} + \mathrm{IIb'} + \mathrm{IIc'} + \mathrm{IIIa'} + \mathrm{IIIb'} + \mathrm{IIIc'}}{\mathrm{Ia} + \mathrm{IIa} + \mathrm{IIIa}}\right) \quad (8)$$

Roman numerals refer to the structures in Fig. 1.

Prior to any residual per soil type inspection, Z-scores and Tukey box plots were used to eliminate all outliers. Once again, only soil types with at least 10 samples after elimination of outliers and samples with missing data were considered.

2.2. Environmental setting in the Mount Fan Si Pan National Park and MAAT modeling

The environmental setting is described in detail by Podwojewski et al. (2011). In short, the Mount Fan Si Pan National Park (22°18′13″3N, 103°46′32″5E) is located in northwestern Vietnam, close to the Chinese border (Fig. 2A). The Fan Si Pan Mountain range is oriented northwest–southeast and culminates at 3143 m above modern sea level, the highest altitude in Vietnam (Podwojewski et al., 2011). The soil bedrock is homogenous throughout the entire mountain range and the anthropic influences are restricted to the foothills, the rest of the mountain range being covered with primary C_3 vegetation that follows a pronounced altitudinal zonation (Fig. 2B; Podwojewski et al., 2011). The Mount Fan Si Pan National Park is subject to a typical monsoonal climate, albeit altered

by altitude and orientation to the winds as air moisture is high all year round with frequent drizzle and fog (Podwojewski et al., 2011).

A linear ordinary least square regression of MAAT vs altitude was established using MAAT data as y values from 17 weather stations in Vietnam and China (Supplementary Table S2) in addition to the Hoang Lien Son Mountain MAAT value as reported in Podwojewski et al. (2011). The obtained slope and intercept were -4.5 ± 0.2 °C/km and 23.2 ± 0.2 °C, the 1-σ root mean square error (RMSE) was 0.6 °C and the *p*-value was much lower than 0.001. The established linear regression was then applied to the Mount Fan Si Pan National Park to derive MAAT at any altitude.

2.3. Fan Si Pan soil profiles and samples

The pedological study of Podwojewski et al. (2011) represented an opportunity to couple brGDGT distributions to soil types, as the latter had already been reliably determined. Ten soil pits had previously been excavated along the Fan Si Pan Mountain by Podwojewski et al. (2011). The soils were initially sampled for soil type characterization – soil organic matter properties and geochemical environment – with respect to environmental changes. Five of the initially investigated soil profiles were selected for this study (FAN 1, FAN 2 and FAN 4 to FAN 6; Fig. 2) as they occur along a well-defined transect (Fig. 2A) and cover the entire pedogenetic sequence (Fig. 2B; Podwojewski et al., 2011). The selected soil profiles and horizons are described in detail by Podwojewski et al. (2011). In

178 short, Podwojewski et al. (2011) described shallow (< 1 m deep) and very
179 acidic soils (3.5–4.7 pH units, measured with a 1:2.5 soil:water ratio) with
180 variable bulk organic carbon (C_{org}) concentrations (0.4–44.1%) and high
181 water content values (40–215%). $\delta^{13}C$ analyses enabled Podwojewski et al.
182 (2011) to confirm C_{org} inputs from dominant C_3 vegetation at every altitude.
183 Podwojewski et al. (2011) also made a floristic inventory at each soil
184 sampling site (Fig. 2B) and distinguished three main climate/vegetation-
185 dependent soil types:

186 (i) Low altitude Acrisols/Alisols – strongly weathered acidic soils with
187 low base saturation at some depth, typical under warm and wet
188 conditions (Podwojewski et al., 2011 and references therein; IUSS
189 Working Group WRB, 2015) – represented by FAN 1 and FAN 2.

190 (ii) Mid-altitude Podzols – acidic soils with an organic layer and an
191 ash-looking eluvial horizon directly underlain by the illuvial *spodic*
192 or Bs horizon due to the accumulation of organo-metallic (Fe, Al)
193 complexes leached by rainwater, typical in cold/temperate forests
194 and in tropical mountain forests (Podwojewski et al., 2011 and
195 references therein; IUSS Working Group WRB, 2015) –
196 represented by FAN 4 and FAN 5.

197 (iii) High altitude Umbrisols – soils with dark topsoil, thick, well-
198 humified and desaturated in the Mount Fan Si Pan National Park,
199 typical under humid conditions with little or no moisture deficit in
200 cool/temperate areas and in (sub)tropical mountain shrub and

grasslands (Podwojewski et al., 2011 and references therein; IUSS Working Group WRB, 2015) – represented by FAN 6.

2.4. Sample preparation and brGDGT analysis

The samples were air dried and sieved through a 2 mm sieve before being ground and homogenized using a mortar and pestle. Between 0.8 and 2.2 g of each sample, depending on C_{org} concentration, was then extracted with DCM:MeOH (9:1, v:v) using an accelerated solvent extractor ASE 350 Dionex at 120 °C and 10^7 Pa. Total lipid extracts were separated following the automated procedure established by Sanchi et al. (2013).

BrGDGT analyses were performed at CEREGE by high-performance liquid chromatography–atmospheric pressure chemical ionization mass spectrometry (HPLC–APCI-MS) using positive ions on a HPLC–MS 1100 Series spectrometer, following Sanchi et al. (2014).

The MBT′ and CBT indices were calculated using equations (5) and (6). Since no local/regional calibration has yet been established for Vietnam, MAAT and pH were estimated using the extended global soil calibration developed by Peterse et al. (2012), equations (1) and (2).

The BIT index was calculated following Hopmans et al. (2004):

$$\mathrm{BIT} = \frac{\mathrm{Ia} + \mathrm{IIa} + \mathrm{IIIa} + \mathrm{IIa'} + \mathrm{IIIa'}}{\mathrm{Cren} + \mathrm{Ia} + \mathrm{IIa} + \mathrm{IIIa} + \mathrm{IIa'} + \mathrm{IIIa'}} \quad (9)$$

Roman numerals refer to the structures in Fig. 1.

Based on duplicate injections of the entire sample set, the mean analytical 1-σ standard deviations (SD, mean of 1-σ SD to individual mean

values) were 0.003 for MBT′, 0.006 for CBT and 0.001 for BIT. These correspond to 0.1 °C and 0.01 pH unit mean analytical uncertainties.

3. Results

3.1. Global MAAT–pH/brGDGT relationships and MAAT–pH residuals per soil type

Twenty-seven different soil types were represented in the 358-component composite global soil dataset (Fig. 3). Visually, the scatters per soil type were not all similar and some soil types such as Luvisols and Regosols were mainly clustered into relatively small MAAT–pH/brGDGT domains and/or comprised a few outliers (Fig. 3 and Supplementary Fig. S1). The composite dataset allowed us to extend the number of soil types suitable for statistical analysis from eight to twelve – from 174 to 298 soil samples. MAAT–pH/brGDGT relationships (Tables 1 and 2) and MAAT(pH) residual distributions (Fig. 4) were thus determined for the most represented soil types only. A few examples of soil types were also selected for more detailed MAAT residual distributions (Fig. 5). The soil samples reconsidered by De Jonge et al. (2014) were used to compare the newest with traditional MAAT–pH/brGDGT relationships per soil type, as well as MAAT(pH) residual distributions per soil type using traditional and newest global soil calibrations (Figs. 4 and 5, Table 2).

Using the composite global soil dataset, five soil types had non-significant MAAT–MBT′/CBT relationships and seven soil types had non-

246 significant pH–CBT relationships (Table 1). For MAAT–MBT′/CBT, the R^2
247 range was 0.0–0.8 and the RMSE range was 2.2–7.0 °C. For pH–CBT, the R^2
248 range was 0.0–0.8 and the RMSE range was 0.4–1.0 pH units (Table 1).
249 Ranges of MAAT–MBT′/CBT coefficients were 46.9 for MBT′ slope, 11.7 for
250 CBT slope and 24.7 for intercept (Table 1). Some pairs of soil types, – for
251 example Andosols and Cambisols – had similar coefficients whereas other
252 pairs of soil types such as Cambisols and Luvisols had at least one
253 coefficient that was significantly different (Table 1). Ranges of pH–CBT
254 coefficients were 2.4 for slope and 3.4 for intercept (Table 1). After the
255 homogeneity of slopes test ($F = 4.83$, $p < 0.001$), pH–CBT slopes per soil type
256 were not all similar. For instance, they were similar between Cambisols and
257 Leptosols, but not between Cambisols and Luvisols (Table 1). When
258 compared to the global MAAT–pH/brGDGT relationships, three soil types
259 had similar MAAT–MBT′/CBT coefficients and three soil types had similar
260 pH–CBT coefficients (Table 1).
261 Using the global soil dataset of De Jonge et al. (2014), two or three
262 soil types had non-significant traditional and new MAAT–pH/brGDGT
263 relationships (Table 2). For MAAT–MBT′/CBT vs MAAT–MBT′$_{5ME}$, the R^2
264 range was 0.1–0.9 vs 0.0–0.9 and the RMSE range was 1.6–6.8 °C vs 2.4–5.6
265 °C. For pH–CBT vs pH–CBT′, the R^2 range was 0.1–0.7 vs 0.0–0.9 and the
266 RMSE range was 0.5–1.1 pH units vs 0.2–0.6 pH units (Table 2). Ranges of
267 MAAT–MBT′/CBT coefficients were 60.6 for MBT′ slope, 10.9 for CBT slope
268 and 22.2 for intercept whereas ranges of MAAT–MBT′$_{5ME}$ coefficients were

46.2 for slope and 34.2 for intercept (Table 2). Ranges of pH–CBT vs pH-CBT′ coefficients were 1.9 vs 1.8 for slope and 3.0 vs 2.8 for intercept (Table 2). For all bivariate traditional and newest MAAT–pH/brGDGT relationships, slopes/intercepts per soil type were not all similar after the homogeneity of slopes tests/ANCOVA (Table 2). When compared to the global MAAT–brGDGT relationships, four soil types had similar MAAT–MBT′/CBT coefficients and six soil types had similar MAAT–MBT′$_{5ME}$ coefficients (Table 2). When compared to the global pH–brGDGT relationships, three soil types had similar pH–CBT coefficients and two soil types had similar pH–CBT′ coefficients (Table 2).

Using the composite global soil dataset, mean MAAT residuals per soil type based on the MAAT–MBT′/CBT global soil calibration of Peterse et al. (2012) varied between –7.0 and 3.5 °C (Figs. 4A, 5A and 5B). Mean pH residuals per soil type based on the pH–CBT global soil calibration of Peterse et al. (2012) varied between –1.3 and 0.4 pH units (data not shown).

Using the global soil dataset of De Jonge et al. (2014), mean MAAT residuals per soil type based on the MAAT–MBT′/CBT global soil calibration of Peterse et al. (2012) varied between –7.5 and 3.5 °C (Figs. 4B, 5C and 5E). Mean MAAT residuals per soil type based on the MAAT–MBT′$_{5ME}$ global soil calibration of De Jonge et al. (2014) varied between –3.5 and 2.5 °C (Figs. 4C, 5D and 5F). Mean pH residuals per soil type based on the pH–CBT global soil calibration of Peterse et al. (2012) varied between –1.4 and 0.2 pH units (data not shown). Mean pH residuals per soil type based on the

292 pH–CBT′ global soil calibration of De Jonge et al. (2014) varied between –0.2
293 and 0.3 pH units (data not shown).
294
295 *3.2. BrGDGT distributions and proxies in the Fan Si Pan National Park*
296 BrGDGTs were present in all Fan Si Pan soil samples. Compounds Ia
297 and IIa/IIa′ were the most abundant in each sample, representing together
298 at least 86% of total brGDGTs (Supplementary Table S3). Conversely,
299 compounds IIIb/IIIb′ and IIIc/IIIc′ were all reliably detected in only one-
300 third of the samples, precluding the use of MBT and associated soil
301 calibrations.
302 BIT, MBT′ and CBT were calculated for all Fan Si Pan soil samples
303 (Fig. 6, Table 3). The BIT range was 0.94–1.00, the MBT′ range was 0.57–
304 0.93 and the CBT range was 1.02–2.01 (Table 3). The MBT′/CBT-based
305 MAAT estimate range was 10.0–20.5 °C using the global soil calibration of
306 Peterse et al. (2012), corresponding to differences with modeled MAAT
307 between –2.8 and 6.2 °C – on average 2.3 ± 1.7 °C (Table 3). The CBT-based
308 pH estimate range was 3.9–5.9 pH units using the global soil calibration of
309 Peterse et al. (2012), corresponding to differences with measured pH
310 between –0.1 and 2.1 pH units – on average 0.9 ± 0.6 pH units (Table 3).
311 BIT varied with depth by maximum 0.04 in all soil profiles (Fig. 6).
312 MBT′ decreased with depth by 0.14–0.21 in Podzols (even if FAN 5 had only
313 three points), looked globally stable in FAN 1 (also with only three points),
314 and was stable in the other soil profiles. CBT was stable in FAN 5,

fluctuated by 0.25–0.50 in FAN 6, and decreased with depth by 0.24–0.66 in the other soil profiles. CBT-based pH variations with depth were opposite and roughly twice as high as CBT variations with depth in all soil profiles. Measured pH increased with depth by 0.5–1.3 pH units in all soil profiles, except FAN 5 with only two points (Fig. 6). However, in FAN 4 and FAN 6, changes in measured pH with depth shifted from decreases in A horizons to increases in B horizons, with variations of 0.2–0.6 pH units in FAN 6 and of 0.4–1.0 pH units in FAN 4. MBT′/CBT-based MAAT decreased with depth by about 4–6 °C in Podzols, increased by about 2.5 °C in Acrisols/Alisols, and was stable in Umbrisols (Fig. 6).

4. Discussion

4.1. Global soil dataset

4.1.1. Soil type diversity and implications for MAAT–pH reconstructions

The 27 soil types represented in the 358-component composite global soil dataset denote its high diversity (Fig. 3 and Supplementary Fig. S1, Supplementary Table S1). Most of the soil samples were taken from surficial and/or A horizons (Supplementary Table S1). Thus, we may assume that soil depth has no significant effect on the global brGDGT distributions considered in this study.

Pedogenetic processes depend on multiple factors such as climate, vegetation type, topography and parent material (e.g., IUSS Working Group WRB, 2015). These differential processes in soil formation and erosion may

have an impact on the production, transformation and preservation of labile substrates for brGDGT producers, including in surficial horizons. Indeed, brGDGT producers are partially attributable to *Acidobacteria* (Weijers et al., 2009; Sinninghe Damsté et al., 2011, 2014) and their metabolism is thought to be the heterotrophic assimilation of labile substrates or the chemoautotrophic consumption of respired CO_2 (Weijers et al., 2010).

Given the specificity of soil types to climatic ranges such as moisture regime/mean annual precipitation (MAP, Fig. 4, Supplementary Table S1), some soil types have small MAAT and/or pH domains that may be associated with small MBT′ and/or CBT domains, which may result in non-significant MAAT–pH/brGDGT relationships (Fig. 3, Table 1 and Supplementary Table S1). For instance, Acrisols, Alisols, Ferralsols, Podzols and Umbrisols did not show a significant pH–CBT anti-correlation, likely due to their typically low pH values and high CBT values (Table 1 and Supplementary S1). Alisols and Ferralsols also had typically high MAAT and MBT′ values, resulting in non-significant MAAT–MBT′/CBT relationships (Table 1 and Supplementary Table S1).

Regression coefficients and performances of MAAT–MBT′/CBT and pH–CBT differed at times between different soil types, whose MAAT–pH/brGDGT relationships were not always similar to global ones (Table 1). After the homogeneity of slopes test, at least one soil type had a significantly different pH–CBT relationship from the others: the wettest and driest soils – Acrisols, Alisols, Ferralsols, Podzols, Regosols and Umbrisols –

could be distinguished from another group comprising Cambisols, Fluvisols and Leptosols based on their pH–CBT slopes and associated standard errors (Table 1). In addition, some soil types such as Alisols, Fluvisols, Phaeozems and Regosols had peculiar MAAT–MBT′/CBT relationships when compared with most other soil types (Table 1). This suggests that high soil heterogeneity has an impact on (acido)bacterial communities involved in brGDGT production (Jones et al., 2009) and that different communities may respond in different ways to environmental changes.

The soil type effect on brGDGTs and their producers is also supported by the different distributions of MAAT residuals per soil type (Fig. 4A), as well as pH residuals per soil type to a lesser extent (data not shown). Six soil types had mainly negative residuals, two soil types had mainly positive residuals and four soil types had roughly equal numbers of positive as negative residuals (Fig. 4A). These three groups of soil types in terms of MAAT residuals were not distinguished by their typical moisture regimes (Fig. 4A, Supplementary Table S1). In addition, some soil types such as Alisols and Podzols had very high MAAT residuals (Figs. 4A, 5A and 5B). Thus, (almost) systematic biases on MAAT–pH reconstructions may occur for a given soil type when using global soil calibrations. This also implies that not all soil types contribute equally to global scatters (Figs. 4A, 5A, 5B and Supplementary Fig. S1).

383 *4.1.2. Traditional vs improved chromatographic method: is there an impact*
384 *on the soil type effect?*

385 Using the soil samples reconsidered by De Jonge et al. (2014), we
386 assess if 5- and 6-methyl brGDGT producers are influenced by the very high
387 soil heterogeneity, following the hypothesis that 5- and 6-methyl brGDGTs
388 are not produced by the same microorganisms (De Jonge et al., 2014).
389 Regression coefficients and performances differed at times between different
390 soil types for traditional and newest MAAT–pH/brGDGT relationships
391 (Table 2). In addition, not all soil types had similar traditional and new
392 MAAT–pH/brGDGT relationships to the global ones. After the homogeneity
393 of slopes tests/ANCOVA, at least one soil type had a significantly different
394 pH–CBT, MAAT–MBT′$_{5ME}$ and pH–CBT′ relationship from the others (Table
395 2). Acrisols, Ferralsols, Podzols and Regosols could be distinguished from
396 Cambisols, Fluvisols and Leptosols by their pH–CBT slopes (Table 2). Some
397 soil types such as Fluvisols and Regosols had peculiar MAAT–MBT′/CBT
398 relationships when compared with most other soil types (Table 2). The main
399 soil types generally had similar MAAT–MBT′$_{5ME}$ slopes, but Fluvisols had a
400 significantly higher intercept than the other soil types (Table 2). Cambisols,
401 Leptosols and Regosols could be distinguished from Fluvisols and Podzols by
402 their pH–CBT′ slopes (Table 2). Thus, the effect of soil type on MAAT–
403 pH/brGDGT relationships remains significant when 5- and 6-methyl
404 brGDGTs are quantified separately.

When considering MAAT–MBT′$_{5ME}$ instead of MAAT–MBT′/CBT per soil type, R^2 changes varied between –0.4 and 0.2, and RMSEs changes varied between –1.2 and 1.1 °C (Table 2). When considering pH–CBT′ instead of pH–CBT per soil type, R^2 changes varied between –0.5 and 0.8, and RMSEs changes varied between –0.7 and 0.0 pH units (Table 2). Therefore, MAAT–pH/brGDGT relationships per soil type – and in particular, MAAT–brGDGT relationships – are not systematically improved when 5- and 6-methyl brGDGTs are quantified separately. In addition, the improvements or deteriorations of MAAT–pH/brGDGT relationships clearly depend on soil type (Table 2).

Decreases in MAAT(pH) residuals per soil type were not very clear when 5- and 6-methyl brGDGTs were quantified separately, except in Regosols (Figs. 4B and 4C). A more detailed inspection of MAAT residual distributions in Leptosols and in Regosols (Fig. 5C and E) revealed that these two soil types had high and opposite MAAT residuals using the MAAT–MBT′/CBT calibration of Peterse et al. (2012). When using the MAAT–MBT′$_{5ME}$ calibration of De Jonge et al. (2014), MAAT residuals of four Regosols decreased much more than the other Regosols and Luvisols (Fig. 5D and F). These four Regosols highlighted by De Jonge et al. (2014) not only had MAP values ≤ 550 mm, but they also had very high 6-methyl brGDGT relative abundances (> 60% of total brGDGTs; Supplementary Table S1). Despite the more substantial MAAT residual reduction in Regosols, MAAT residual distributions per soil type were still not all

similar, as there remained some soil types with high and/or mainly positive or negative residuals (Fig. 4C).

Averaged MAP values per soil type varied between 472 and 1870 mm, which suggests that moisture regime clearly depends on soil type. Likewise, averaged soil pH values per soil type varied between 4.4 and 7.3 pH units, whereas averaged 6-methyl brGDGT relative abundances per soil type varied between 1.4 and 51.7% of total brGDGTs (Supplementary Table S1). Regosols had on average the lowest MAP values, and the highest pH values and 6-methyl brGDGT relative abundances (Supplementary Table S1), which is consistent with the greatest improvement of their pH–brGDGT relationship and the greatest decreases in MAAT(pH) residuals (Fig. 4B and C, Table 2). Conversely, soil types with averaged MAP values > 1000 mm had the lowest averaged pH values and 6-methyl brGDGT relative abundances (Supplementary Table S1), so no improvement of MAAT–pH/brGDGT relationships nor clear decrease in MAAT(pH) residuals was expected. However, pH–brGDGT relationships were improved in the wettest soils (Fig. 4B and C, Table 2). In addition, soil types with averaged MAP values between 500 and 1000 mm showed no intermediate behaviors between the wettest and the driest soils (Fig. 4B and C, Table 2). This likely explains why the separate quantification of 5- and 6-methyl brGDGTs barely reduces the soil type effect on brGDGTs.

4.2. Fan Si Pan soil transect

451 *4.2.1. BrGDGT-derived proxies*

452 BIT values in Fan Si Pan soils (Table 3) are close to the reported
453 mean soil BIT value of 0.90 ± 0.14 (Schouten et al., 2013) and are consistent
454 with those observed in wet and acidic soils (e.g., Weijers et al., 2006b;
455 Loomis et al., 2011; Dirghangi et al., 2013). For MAAT, only one Fan Si Pan
456 soil fell outside the global MAAT–MBT′/CBT RMSE of Peterse et al. (2012)
457 of 5 °C (Table 3). For pH, half of the Fan Si Pan soils fell outside the global
458 pH–CBT RMSE of Peterse et al. (2012) of 0.8 pH units (Table 3). As RSME
459 means that globally 66% of the soils will fall within this error range, Fan Si
460 Pan soils adhere quite well to the variabilities of the global soil calibration
461 dataset of Peterse et al. (2012), especially for MAAT–MBT′/CBT.

462 The absence of correlation between measured pH and CBT (r = –0.11,
463 p = 0.67, Fig. 6) when all Fan Si Pan soils are considered together is likely
464 due to their very small pH domain (3.5–4.7 pH units, Table 3) and/or to the
465 differential relationships per soil type (Fig. 6, Table 3). Indeed, CBT and
466 measured pH were anti-correlated in Acrisols/Alisols, positively correlated
467 in Umbrisols, and had no clear relationship in Podzols.

468 MAAT–pH reconstructions along the Fan Si Pan transect may be
469 substantially biased by the co-elution of 5- and 6-methyl brGDGTs due to
470 our chromatographic method. Indeed, Yang et al. (2015a) have shown that
471 6-methyl brGDGTs significantly deteriorate the performance of MBT′ as a
472 MAAT/altitude proxy along Mt. Shennongjia, China. Additionally, MBT′ is
473 not (well) correlated with MAAT/altitude along most other altitudinal

transects studied so far in China, India and Tanzania (Peterse et al., 2009b; Yang et al., 2010; Ernst et al., 2013; Coffinet et al., 2014; Deng et al., 2016), which may be due to 6-methyl brGDGTs as well. Conversely, soil depth effect is not a plausible explanation as the soil samples considered for altitudinal lapse rate studies were taken from surficial horizons.

4.2.2. Soil type effect on brGDGTs: a focus on contrasting soil organic matter properties

For the Fan Si Pan surficial soils – sampled from horizons with a mean soil depth < 10 cm – MBT′ and MBT′/CBT-based MAAT mainly decreased between the lowest and highest altitude soils, in particular between the Podzols FAN4.1/FAN5.1 and the Umbrisols FAN6.1/FAN6.2 (Fig. 6, Table 3). Conversely, MAAT estimates did not decrease with altitude between the Acrisol FAN1.1, the Alisols FAN2.A0/FAN2.1 and the Podzol FAN4.1. Despite our difficulties in separating the effects of vegetation/soil type and adiabatic cooling on brGDGT distributions along the Fan Si Pan transect, the absence of a decrease in MAAT estimates between the four lowest altitude soils suggests the importance of the diversity of soils encountered along this transect.

The different main soil types present along the Fan Si Pan transect have contrasting C_{org} sources, stocks and mineralization rates (Podwojewski et al., 2011). In the Fan Si Pan Acrisols, C_{org} has a rapid turnover due to relatively high temperatures and constant inputs from leaves, resulting in a

497 thin litter layer and rapid C_{org} mineralization. In the Fan Si Pan Podzols,
498 C_{org} decomposition rate is lower, partially due to cooler temperatures and
499 seasonal inputs from leaves (Podwojewski et al., 2011). The Fan Si Pan
500 Podzols thus have a thicker litter layer, resulting in very high topsoil C_{org}
501 stocks. In addition, the second major change in vegetation type along the
502 Fan Si Pan transect has induced the transition from Podzols to Umbrisols
503 with a thinning of the litter layer, resulting in lower topsoil C_{org} stocks and a
504 different C_{org} source (Fig. 2B; Podwojewski et al., 2011). Indeed, C_{org} inputs
505 for Podzols are exogenic – mainly from the thick litter layer – whereas C_{org}
506 inputs for Umbrisols are endogenic, mainly from bamboo roots and thus
507 more homogenous.

508 Substantial changes in C_{org} sources, stocks and/or mineralization
509 rates in soils may induce changes in substrate nature and/or nutrient
510 availability for brGDGT producers, which may modify brGDGT distributions
511 and so bias MAAT–pH reconstructions, as suggested by previous workers
512 such as Anderson et al. (2014). Thus, biases due to vegetation and soil types
513 should be jointly investigated, preferentially along lateral and local soil
514 transects with as many constant environmental parameters as possible,
515 such as MAAT, soil temperature, vegetation type and parent material.

516

517 *4.2.3. Effects of soil depth on brGDGT-derived proxies*

518 The soil collection of the Fan Si Pan transect allows to investigate five
519 well-studied soil profiles. Substantially lower brGDGT-based MAATs in

deep soils as opposed to topsoils were reported in two Podzol profiles under different climates (Huguet et al., 2010), a trend that also occurred in the Fan Si Pan Podzol profiles, but not in the other Fan Si Pan soil profiles (Fig. 6). Likewise, changes in CBT-based pH with depth were not similar between the different Fan Si Pan soil profiles (Fig. 6). We do not know to what extent (acido)bacterial communities change with depth in the different Fan Si Pan soil profiles nor to what extent such changes impact brGDGT distributions in soils. For this reason, we put forward various explanations for the observed changes in brGDGT distributions with soil depth.

Every Fan Si Pan sample was 2-mm sieved (Podwojewski et al., 2011), meaning that root-associated brGDGTs in subsoils (Huguet et al., 2013b) cannot explain the decreased MAAT estimates in the deep Fan Si Pan Podzols. Nevertheless, given that bamboo roots (abundant in the Umbrisol profile FAN 6) are more mineralizable than tree roots (abundant in the Podzol profiles FAN 4 and FAN 5), brGDGT producing communities may change differently with depth between the main Fan Si Pan soil types, resulting in differential associated biases on MAAT–pH estimates, following the hypothesis that different (acido)bacterial species do not all produce the same brGDGTs (Sinninghe Damsté et al., 2011, 2014; De Jonge et al., 2014). Alternatively, Podzols have the peculiarity of having a subsoil enriched in Fe, Al and organic matter – including lipids – due to rainwater percolation (e.g., Huguet et al., 2010; Podwojewski et al., 2011). Therefore, substantial changes with depth in biotic and abiotic processes not related to brGDGT

543 producers – for instance, lipid transfer to a non-extractable pool via organo-
544 metallic complexation – may occur in podzol soils (e.g., Huguet et al., 2010).
545 Nevertheless, such processes – which also include soil bioturbation by soil
546 fauna and soil reworking by rooted trees – are unlikely to be restricted to
547 Podzols.

548 BrGDGT distributions may also be influenced by the history of the
549 soils. Former agricultural activities – mainly maize crops (Fig. 2B;
550 Podwojewski et al., 2011) – may have impacted brGDGT distributions in the
551 FAN 1 soil profile. Additionally, the transition from primary broad-leaved
552 forests to alpine vegetation (Fig. 2B; Podwojewski et al., 2011) has shifted
553 upwards in altitude under the effect of the present global warming (IPCC,
554 2013). This transition is now close to the FAN 6 site, which may thus have
555 experienced a major temporal change in vegetation type. However, the
556 brGDGT turnover times reported so far – from a few months to less than 45
557 years (Peterse et al., 2010; Weijers et al., 2010; Huguet et al., 2013a) – may
558 be true for surficial soils only. Indeed, brGDGTs may be associated with the
559 mineral phase and/or be incorporated within the macromolecular matrix in
560 deeper soil horizons (e.g., Huguet et al., 2010), whereas microbial activity
561 may decrease with depth, resulting in substantially longer brGDGT
562 turnover times in deep soils. The latter is suggested by decreases in C_{org}-
563 normalized brGDGT absolute abundances with depth in FAN 1, FAN 2 and
564 FAN 4 (data not shown). Additionally, imprints of former communities may
565 be muted by the post-depositional effect (e.g., Zech et al., 2012; Yamamoto et

566 al., 2016), and such an effect is indeed suggested by an increase in C_{org}-
567 normalized brGDGT absolute abundances with depth in FAN 6 (data not
568 shown).
569
570 **5. Conclusions and perspectives**
571 Soil types were assigned to a composite global dataset of 358 soils to
572 investigate MAAT–pH/brGDGT relationships and MAAT(pH) residuals per
573 soil type. Distributions of brGDGTs were also investigated in five soil
574 profiles excavated along an altitudinal transect in the Mount Fan Si Pan
575 National Park. Surrounding vegetation, geological setting, as well as soil
576 sequence had previously been intensively characterized, providing an
577 opportunity to investigate their impact on proxies intensively used in paleo-
578 studies.
579 The soil type diversity of the global dataset was high, traditional
580 MAAT–pH/relationships per soil type were not all similar and different soil
581 types (e.g., Alisols and Podzols) did not all provide the same contribution to
582 global MAAT(pH)/brGDGT scatters. Additionally, the soil type effect on
583 MAAT–pH relationships remained significant when 5- and 6-methyl
584 brGDGTs were quantified separately and no obvious reduction in
585 MAAT(pH) residuals per soil type occurred in general (e.g., in Leptosols,
586 which contained 6-methyl brGDGTs). In the Mount Fan Si Pan National
587 Park, MBT′/CBT-based MAATs were not significantly different to modeled
588 MAATs when the global calibration error of 5 °C was taken into account.

However, the decrease in MAAT estimates along the altitudinal transect lacked clarity when the focus was on surficial soils, and the pH–CBT relationship was absent when all Fan Si Pan soils were considered. On the one hand, substantial changes in soil/vegetation type along the Fan Si Pan transect may induce biases on MAAT–pH reconstructions in surficial soils. On the other hand, MBT′/CBT indices varied slightly or substantially with depth in the Fan Si Pan soil profiles, possibly as a function of soil type and history.

To better understand the biases on brGDGT-based estimates, more soil profiles should be investigated along topo-sequences, as attempted in our work. Indeed, this study reveals the importance of direct collaborations between organic geochemists and pedologists, ensuring that specific organic compounds and physico-chemical soil properties are jointly investigated. To consider the evolution of soil properties through time, as well as the transfer time of soil C_{org}, radiocarbon analyses on bulk soil C_{org} and on specific organic compounds should be conducted. Additionally, future global/regional/local soil MAAT–pH/brGDGT calibrations should consider sample sizes of a few dozen to a few hundred per soil type to ensure adequate specificity for all given soil types.

Acknowledgements

G.M. thanks Anneke de Rouw and the HYDRARIDE consortium for making this study and the connection with pedologists possible through

612 discussions in the field in Cameroon. Work at CEREGE is supported by
613 ECCOREV FR3098 (project ECCOTEMP) and the Collège de France. N.D.
614 thanks Ecole Normale Supérieure de Lyon for providing salary support. We
615 are grateful to two anonymous reviewers for their constructive suggestions
616 that greatly helped us to considerably improve this manuscript.
617
618 **Appendix A. Supplementary material.**
619
620 *Associate Editor*–**Klaas Nierop**
621
622 **References**
623 Anderson, V.J., Shanahan, T.M., Saylor, J.E., Horton, B.K., Mora, A.R.,
624 2014. Sources of local and regional variability in the MBT′/CBT
625 paleotemperature proxy: Insights from a modern elevation transect
626 across the Eastern Cordillera of Colombia. Organic Geochemistry 69,
627 42–51.
628 Coffinet, S., Huguet, A., Williamson, D., Fosse, C., Derenne, S., 2014.
629 Potential of GDGTs as a temperature proxy along an altitudinal
630 transect at Mount Rungwe (Tanzania). Organic Geochemistry 68, 82–
631 89.
632 Dang, X., Yang, H., Naafs, B.D.A., Pancost, R.D., Xie, S., 2016. Evidence of
633 moisture control on the methylation of branched glycerol dialkyl

glycerol tetraethers in semi-arid and arid soils. Geochimica et Cosmochimica Acta 189, 24–36.

De Jonge, C., Hopmans, E.C., Zell, C.I., Kim, J.-H., Schouten, S., Sinninghe Damsté, J.S., 2014. Occurrence and abundance of 6-methyl branched glycerol dialkyl glycerol tetraethers in soils: Implications for palaeoclimate reconstruction. Geochimica et Cosmochimica Acta 141, 97–112.

Deng, L., Jia, G., Jin, C., Li, S., 2016. Warm season bias of branched GDGT temperature estimates causes underestimation of altitudinal lapse rate. Organic Geochemistry 96, 11–17.

Dirghangi, S.S., Pagani, M., Hren, M.T., Tipple, B.J., 2013. Distribution of glycerol dialkyl glycerol tetraethers in soils from two environmental transects in the USA. Organic Geochemistry 59, 49–60.

Ernst, N., Peterse, F., Breitenbach, S.F.M., Syiemlieh, H.J., Eglinton, T.I., 2013. Biomarkers record environmental changes along an altitudinal transect in the wettest place on Earth. Organic Geochemistry 60, 93–99.

Fox, J., Weisberg, S., 2011. An {R} Companion to Applied Regression, Second edition. Sage, Thousand Oaks CA, USA. http://socserv.socsci.mcmaster.ca/jfox/Books/Companion.

Hengl, T., de Jesus, J.M., MacMillan, R.A., Batjes, N.H., Heuvelink, G.B.M., Ribeiro, E., Samuel-Rosa, A., Kempen, B., Leenaars, J.G.B., Walsh,

656 M.G., Gonzalez, M.R., 2014. SoilGrids1km — Global soil information
657 based on automated mapping. PLoS ONE 9, e105992.
658 Hopmans, E.C., Weijers, J.W.H., Schefuß, E., Herfort, L., Sinninghe
659 Damsté, J.S., Schouten, S., 2004. A novel proxy for terrestrial organic
660 matter in sediments based on branched and isoprenoid tetraether
661 lipids. Earth and Planetary Science Letters 224, 107–116.
662 Huguet, A., Fosse, C., Metzger, P., Fritsch, E., Derenne, S., 2010.
663 Occurrence and distribution of extractable glycerol dialkyl glycerol
664 tetraethers in podzols. Organic Geochemistry 41, 291–301.
665 Huguet, A., Fosse, C., Laggoun-Défarge, F., Delarue, F., Derenne, S., 2013a.
666 Effects of a short-term experimental microclimate warming on the
667 abundance and distribution of branched GDGTs in a French
668 peatland. Geochimica et Cosmochimica Acta 105, 294–315.
669
670 Huguet, A., Gocke, M., Derenne, S., Fosse, C., Wiesenberg, G.L.B., 2013b.
671 Root-associated branched tetraether source microorganisms may
672 reduce estimated paleotemperatures in subsoil. Chemical Geology
673 356, 1–10.
674 IPCC, 2013. Climate change 2013: The physical science basis. Contribution
675 of Working Group I to the Fifth Assessment Report of the
676 Intergovernmental Panel on Climate Change [Stocker, T.F., Qin, D.,
677 Plattner, G.-K., Tignor, M., Allen, S.K., Boschung, J., Nauels, A., Xia,

678 Y., Bex, V., Midgley, P.M. (eds.)]. Cambridge University Press,
679 Cambridge, United Kingdom and New York, NY, USA.
680 IUSS Working Group WRB, 2015. World Reference Base for Soil Resources
681 2014, update 2015. International soil classification system for naming
682 soils and creating legends for soil maps. World Soil Resources Reports
683 No. 106. FAO, Rome.
684 Jones, R.T., Robeson, M.S., Lauber, C.L., Hamady, M., Knight, R., Fierer,
685 N., 2009. A comprehensive survey of soil acidobacterial diversity
686 using pyrosequencing and clone library analyses. The ISME Journal
687 3, 442–453.
688 Liu, W., Wang, H., Zhang, C.L., Liu, Z., He, Y., 2013. Distribution of glycerol
689 dialkyl glycerol tetraether lipids along an altitudinal transect on Mt.
690 Xiangpi, NE Qinghai-Tibetan Plateau, China. Organic Geochemistry
691 57, 76–83.
692 Loomis, S.E., Russell, J.M., Sinninghe Damsté, J.S., 2011. Distributions of
693 branched GDGTs in soils and lake sediments from western Uganda:
694 Implications for a lacustrine paleothermometer. Organic
695 Geochemistry 42, 739–751.
696 Menges, J., Huguet, C., Alcañiz, J.M., Fietz, S., Sachse, D., Rosell-Melé, A.,
697 2014. Influence of water availability in the distributions of branched
698 glycerol dialkyl glycerol tetraether in soils of the Iberian Peninsula.
699 Biogeosciences 11, 2571–2581.

Nieto-Moreno, V., Rohrmann, A., van der Meer, M.T.J., Sinninghe Damsté, J.S., Sachse, D., Tofelde, S., Niedermeyer, E.M., Strecker, M.R., Mulch, A., 2016. Elevation-dependent changes in *n*-alkane δD and soil GDGTs across the South Central Andes. Earth and Planetary Science Letters (in press). http://dx.doi.org/10.1016/j.epsl.2016.07.049.

Peterse, F., Nicol, G.W., Schouten, S., Sinninghe Damsté, J.S., 2010. Influence of soil pH on the abundance and distribution of core and intact polar lipid-derived branched GDGTs in soil. Organic Geochemistry 41, 1171–1175.

Peterse, F., Schouten, S., van der Meer, M.T.J., Sinninghe Damsté, J.S., 2009a. Distribution of branched tetraether lipids in geothermally heated soils: Implications for the MBT/CBT temperature proxy. Organic Geochemistry 40, 201–205.

Peterse, F., van der Meer, M.T.J., Schouten, S., Jia, G., Ossebaar, J., Blokker, J., Sinninghe Damsté, J.S., 2009b. Assessment of soil *n*-alkane δD and branched tetraether membrane lipid distributions as tools for paleoelevation reconstruction. Biogeosciences 6, 2799–2807.

Peterse, F., van der Meer, J., Schouten, S., Weijers, J.W.H., Fierer, N., Jackson, R.B., Kim, J.-H., Sinninghe Damsté, J.S., 2012. Revised calibration of the MBT–CBT paleotemperature proxy based on branched tetraether membrane lipids in surface soils. Geochimica et Cosmochimica Acta 96, 215–229.

722 Podwojewski, P., Poulenard, J., Nguyet, M.L., de Rouw, A., Nguyen, V.T.,
723 Pham, Q.H., Tran, D.T., 2011. Climate and vegetation determine soil
724 organic matter status in an alpine inner-tropical soil catena in the
725 Fan Si Pan Mountain, Vietnam. Catena 87, 226–239.
726 R Development Core Team, 2016. R: A language and environment for
727 statistical computing. R Foundation for Statistical Computing,
728 Vienna, Austria. ISBN 3-900051-07-0, url: http://www.R-project.org.
729 Sanchi, L., Ménot, G., Bard, E., 2014. Insights into continental
730 temperatures in the northwestern Black Sea area during the Last
731 Glacial period using branched tetraether lipids. Quaternary Science
732 Reviews 84, 98–108.
733 Sanchi, L., Ménot, G., Bard, E., 2013. An automated purification method for
734 archaeal and bacterial tetraethers in soils and sediments. Organic
735 Geochemistry 54, 83–90.
736 Schouten, S., Hopmans, E.C., Sinninghe Damsté, J.S., 2013. The organic
737 geochemistry of glycerol dialkyl glycerol tetraether lipids: A review.
738 Organic Geochemistry 54, 19–61.
739 Sinninghe Damsté, J.S., Ossebaar, J., Schouten, S., Verschuren, D., 2008.
740 Altitudinal shifts in the branched tetraether lipid distribution in soil
741 from Mt. Kilimanjaro (Tanzania): Implications for the MBT/CBT
742 continental palaeothermometer. Organic Geochemistry 39, 1072–
743 1076.

744 Sinninghe Damsté, J.S., Rijpstra, W.I.C., Hopmans, E.C., Foesel, B.U.,
745 Wüst, P.K., Overmann, J., Tank, M., Bryant, D.A., Dunfield, P.F.,
746 Houghton, K., Stott, M.B., 2014. Ether- and ester-bound *iso*-diabolic
747 acid and other lipids in members of *Acidobacteria* subdivision 4.
748 Applied and Environmental Microbiology 80, 5207–5218.
749 Sinninghe Damsté, J.S., Rijpstra, W.I.C., Hopmans, E.C., Weijers, J.W.H.,
750 Foesel, B.U., Overmann, J., Dedysh, S.N., 2011. 13,16-Dimethyl
751 octacosanedioic acid (*iso*-diabolic acid), a common membrane-
752 spanning lipid of *Acidobacteria* subdivisions 1 and 3. Applied and
753 Environmental Microbiology 77, 4147–4154.
754 Smerdon, J.E., Pollack, H.N., Cermak, V., Enz, J.W., Kresl, M., Safanda, J.,
755 Wehmiller, J.F., 2004. Air-ground temperature coupling and
756 subsurface propagation of annual temperature signals. Journal of
757 Geophysical Research 109, D21107.
758 Wang, H., Liu, W., Lu, H., 2016. Appraisal of branched glycerol dialkyl
759 glycerol tetraether-based indices for North China. Organic
760 Geochemistry 98, 118–130.
761
762 Weijers, J.W.H., Schouten, S., Hopmans, E.C., Geenevasen, J.A.J., David,
763 O.R.P., Coleman, J.M., Pancost, R.D., Sinninghe Damsté, J.S., 2006a.
764 Membrane lipids of mesophilic anaerobic bacteria thriving in peats
765 have typical archaeal traits. Environmental Microbiology 8, 648–657.

766 Weijers, J.W.H., Schouten, S., Spaargaren, O.C., Sinninghe Damsté, J.S.,
767 2006b. Occurrence and distribution of tetraether membrane lipids in
768 soils: Implications for the use of the TEX_{86} proxy and the BIT index.
769 Organic Geochemistry 37, 1680–1693.
770 Weijers, J.W.H., Schouten, S., van den Donker, J.C., Hopmans, E.C.,
771 Sinninghe Damsté, J.S., 2007. Environmental controls on bacterial
772 tetraether membrane lipid distribution in soils. Geochimica et
773 Cosmochimica Acta 71, 703–713.
774 Weijers, J.W.H., Panoto, E., van Bleijswijk, J., Schouten, S., Rijpstra,
775 W.I.C., Balk, M., Stams, A.J.M., Sinninghe Damsté, J.S., 2009.
776 Constraints on the biological source(s) of the orphan branched
777 tetraether membrane lipids. Geomicrobiology Journal 26, 402–414.
778 Weijers, J.W.H., Wiesenberg, G.L.B., Bol, R., Hopmans, E.C., Pancost, R.D.,
779 2010. Carbon isotopic composition of branched tetraether membrane
780 lipids in soils suggest a rapid turnover and a heterotrophic life style
781 of their source organism(s). Biogeosciences 7, 2959–2973.
782 Yamamoto, Y., Ajioka, T., Yamamoto, M., 2016. Climate reconstruction
783 based on GDGT-based proxies in a paleosol sequence in Japan:
784 Postdepositional effect on the estimation of air temperature.
785 Quaternary International 397, 380–391.
786 Yang, H., Ding, W., He, G., Xie, S., 2010. Archaeal and bacterial tetraether
787 membrane lipids in soils of varied altitudes in Mt. Jianfengling in
788 South China. Journal of Earth Science 21, 277–280.

789 Yang, H., Lü, X., Ding, W., Lei, Y., Dang, X., Xie, S., 2015a. The 6-methyl
790 branched tetraethers significantly affect the performance of the
791 methylation index (MBT′) in soils from an altitudinal transect at
792 Mount Shennongjia. Organic Geochemistry 82, 42–53.
793 Yang, H., Xiao, W., Jia, C., Xie, S., 2015b. Paleoaltimetry proxies based on
794 bacterial branched tetraether membrane lipids in soils. Frontiers of
795 Earth Science 9, 13–25.
796 Zech, R., Gao, L., Tarozo, R., Huang, Y., 2012. Branched glycerol dialkyl
797 glycerol tetraethers in Pleistocene loess-paleosol sequences: Three
798 case studies. Organic Geochemistry 53, 38–44.
799 Zhuang, G., Pagani, M., Chamberlin, C., Strong, D., Vandergoes, M., 2015.
800 Altitudinal shift in stable hydrogen isotopes and microbial tetraether
801 distribution in soils from the Southern Alps, NZ: Implications for
802 paleoclimatology and paleoaltimetry. Organic Geochemistry 79, 56–
803 64.
804

805 **Figure captions**

806 **Fig. 1.** Structures of crenarchaeol (Cren), 5-methyl (Roman numbers with
807 no prime symbol) and 6-methyl (Roman numbers with a prime symbol)
808 branched glycerol dialkyl glycerol tetraethers (brGDGTs, I-II-III) with the
809 different α5 and/or ω5 positions and the different α6 and/or ω6 positions of
810 the methyl groups.

811

812 **Fig. 2.** (A) Maps showing the locations of the study site (left-hand map) and
813 the studied soil profiles (right-hand map). Contour interval is 200 m and
814 contour lines indicate altitudes between 1000 and 3000 m on the right-hand
815 map, with darker tones for higher altitudes. Modified from maps generated
816 from GeoMapApp (http://www.geomapapp.org). (B) Profile showing the
817 studied soil pits. Altitudinal zonation of vegetation types is indicated in
818 green. The profile does not pass exactly through the soil pits, which explains
819 why their altitudes in the profile do not correspond to their actual altitudes.
820 Horizons are delimited and color-coded as per the samples taken by
821 Podwojewski et al. (2011): orange-yellow tones for A horizons, blue tones for
822 Bw horizons and green tones for Bs horizons. Like tones correspond to like
823 horizons. The horizons considered for soil brGDGT distributions are
824 indicated in red. Adapted from Podwojewski et al. (2011).

825

826 **Fig. 3.** BrGDGT-derived proxy data from the composite global soil dataset
827 (Huguet et al., 2010; Peterse et al., 2012; Dirghangi et al., 2013; Anderson et

al., 2014; De Jonge et al., 2014), with 27 soil types being distinguished. (A) Instrumental/modeled mean annual air temperature (MAAT) vs MBT′/CBT. (B) Instrumental/modeled MAAT vs MBT'_{5ME}. (C) Measured pH vs CBT. (D) Measured pH vs CBT′. The outliers are also shown in each plot. The red lines in plots (B), (C) and (D) correspond to the global linear regressions on the composite global soil dataset after outlier removal.

Fig. 4. Box-whisker plots of mean annual air temperature (MAAT) residuals per soil type showing minima and maxima with whiskers, medians with horizontal bars, 1st and 3rd quartiles with boxes, and means with pluses. Plot (A) is based on the composite global soil dataset (Huguet et al., 2010; Peterse et al., 2012; Dirghangi et al., 2013; Anderson et al., 2014; De Jonge et al., 2014). Plots (B) and (C) are based on the soils reconsidered by De Jonge et al. (2014). In plots (A) and (B), residuals are based on the MAAT–MBT′/CBT global soil calibration of Peterse et al. (2012). In plot (C), residuals are based on the MAAT–MBT'_{5ME} global soil calibration of De Jonge et al. (2014). Only soil types comprising at least 10 soils from the global datasets are considered. When outliers are identified for a given soil type, their number is indicated as (initial number of samples – number of outliers) below the number of samples actually considered. Moisture regimes based on averaged mean annual precipitation (MAP) values per soil type are specified with the following color-coding of the numbers of samples

per soil type: blue if MAP > 1000 mm, orange if MAP 500–1000 mm and red if MAP < 500 mm.

Fig. 5. Mean annual air temperature (MAAT) residual distributions for (A) Podzols, (B) Alisols, (C) and (D) Leptosols, and (E) and (F) Regosols. Plots (A) and (B) are based on the composite global soil dataset (Huguet et al., 2010; Peterse et al., 2012; Dirghangi et al., 2013; Anderson et al., 2014; De Jonge et al., 2014). Plots (C), (D), (E) and (F) are based on the soils reconsidered by De Jonge et al. (2014). In plots (A), (B), (C) and (E), residuals are based on the MAAT–MBT′/CBT global soil calibration of Peterse et al. (2012). In plots (D) and (F), residuals are based on the MAAT–MBT'_{5ME} global soil calibration of De Jonge et al. (2014). Gaussians indicate the mean values with their standard deviations. Filled circles represent the medians and filled diamonds represent the extreme values and the 1st and 3rd quartiles. When outliers are identified for a given soil type, their number is indicated as (initial number of samples – number of outliers) below the number of samples actually considered.

Fig. 6. BIT (Hopmans et al., 2004), MBT′ (Peterse et al., 2012), CBT (Weijers et al., 2007), and MBT′/CBT-derived mean annual air temperature (MAAT) and pH based on the extended soil calibration (Peterse et al., 2012) in the studied Fan Si Pan soil profiles. Modeled MAAT and measured pH (Podwojewski et al., 2011 for the latter) are shown for comparison. Horizons

are delimited and color-coded as described in the caption for Fig. 2B. Symbols with error bars next to axis titles represent mean 1-σ standard deviations to mean values of duplicates. Surficial horizons, with a mean depth < 10 cm, are indicated in red.

Table captions

Table 1

Number of samples (n), coefficients (a, b, c, S, I and R^2), and root mean square errors (E) of traditional mean annual air temperature (MAAT)–pH/brGDGT linear regressions per soil type using the composite global soil dataset (Huguet et al., 2010; Peterse et al., 2012; Dirghangi et al., 2013; Anderson et al., 2014; De Jonge et al., 2014). Only soil types comprising at least 10 soils from the global dataset are considered for the linear regressions. When outliers are identified for a given MAAT–pH/brGDGT relationship per soil type, their number is indicated as (initial number of samples – number of outliers) next to the number of samples actually considered. Statistical significance is reached for p-values < 0.05.

Table 2

Number of samples (n), coefficients (a, b, c, S, I and R^2), and root mean square errors (E) of traditional and newest mean annual air temperature (MAAT)–pH/brGDGT linear regressions per soil type using the soils of the composite global soil dataset (Huguet et al., 2010; Peterse et al., 2012;

Dirghangi et al., 2013; Anderson et al., 2014; De Jonge et al., 2014) reconsidered by De Jonge et al. (2014). Only soil types comprising at least 10 soils from the global dataset are considered for the linear regressions. When outliers are identified for a given MAAT–pH/brGDGT relationship per soil type, their number is indicated as (initial number of samples – number of outliers) next to the number of samples actually considered. Statistical significance is reached for p-values < 0.05.

Table 3

BrGDGT-derived proxies and MBT′/CBT-derived mean annual air temperature (MAAT) and pH based on the extended soil calibration (Peterse et al., 2012) along the Fan Si Pan Mountain transect. Altitude, coordinates, horizon, mean depth, organic carbon (C_{org}) concentration, water content (H_2O), and measured pH are from Podwojewski et al. (2011). nd = not determined.

Figure 1

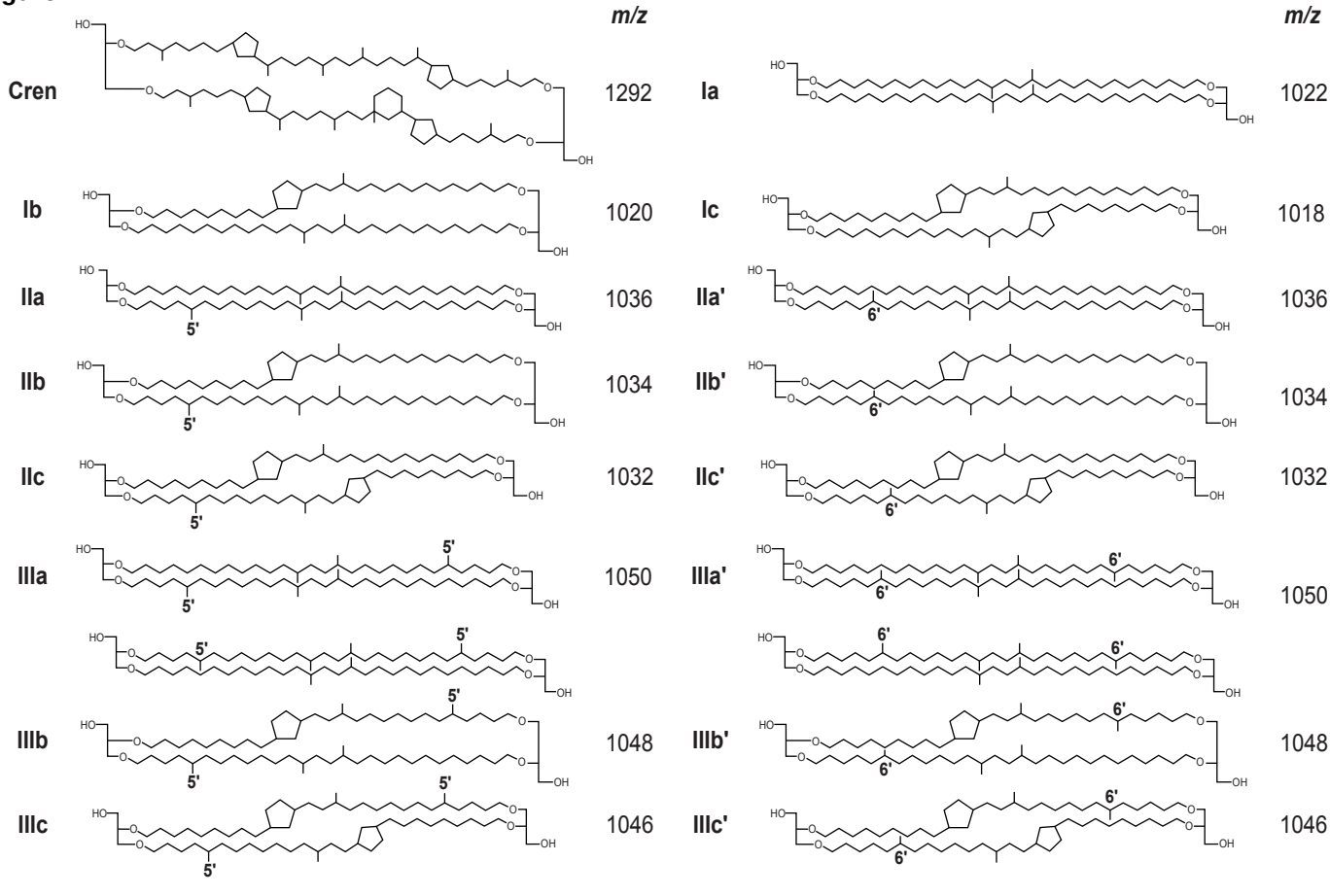
m/z
Cren
1292
Ia
1022
Ib
1020
Ic
1018
IIa
1036
IIa'
1036
IIb
1034
IIb'
1034
IIc
1032
IIc'
1032
IIIa
1050
IIIa'
1050
IIIb
1048
IIIb'
1048
IIIc
1046
IIIc'
1046

Figure 2 - revised

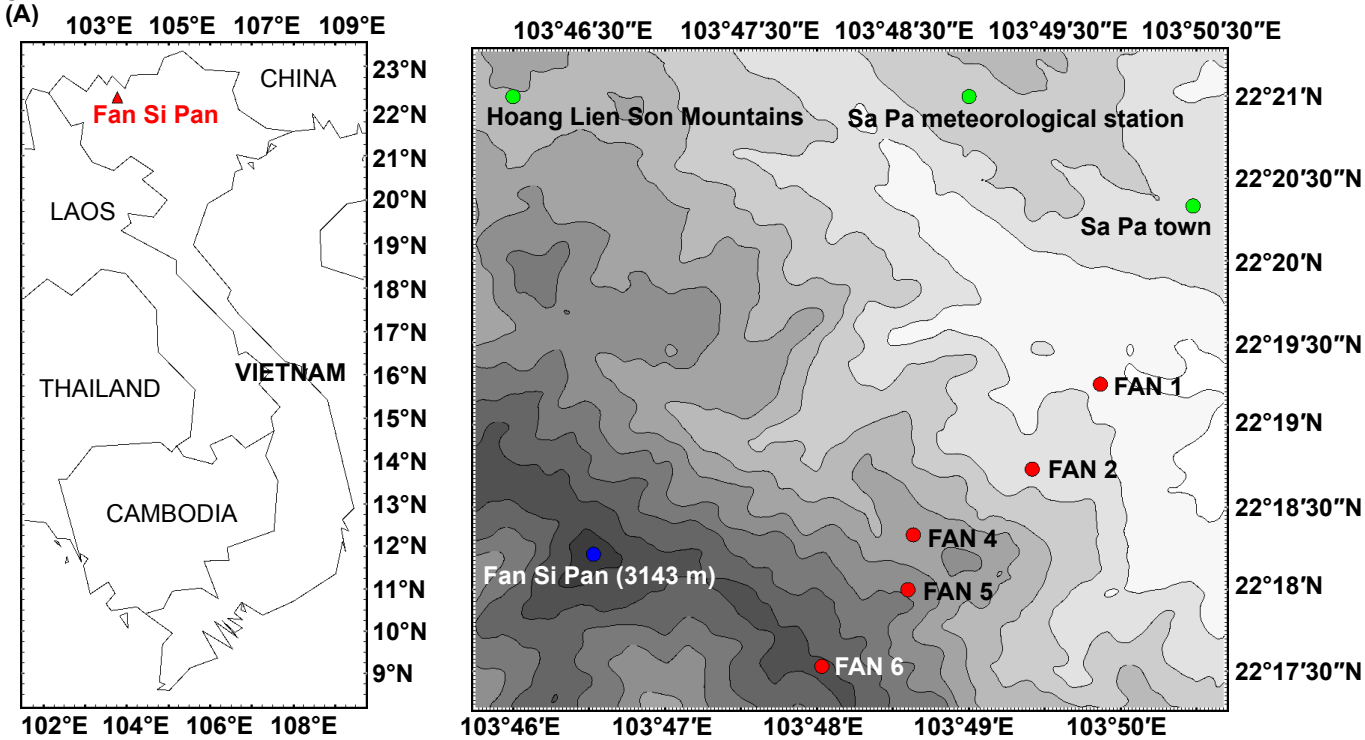

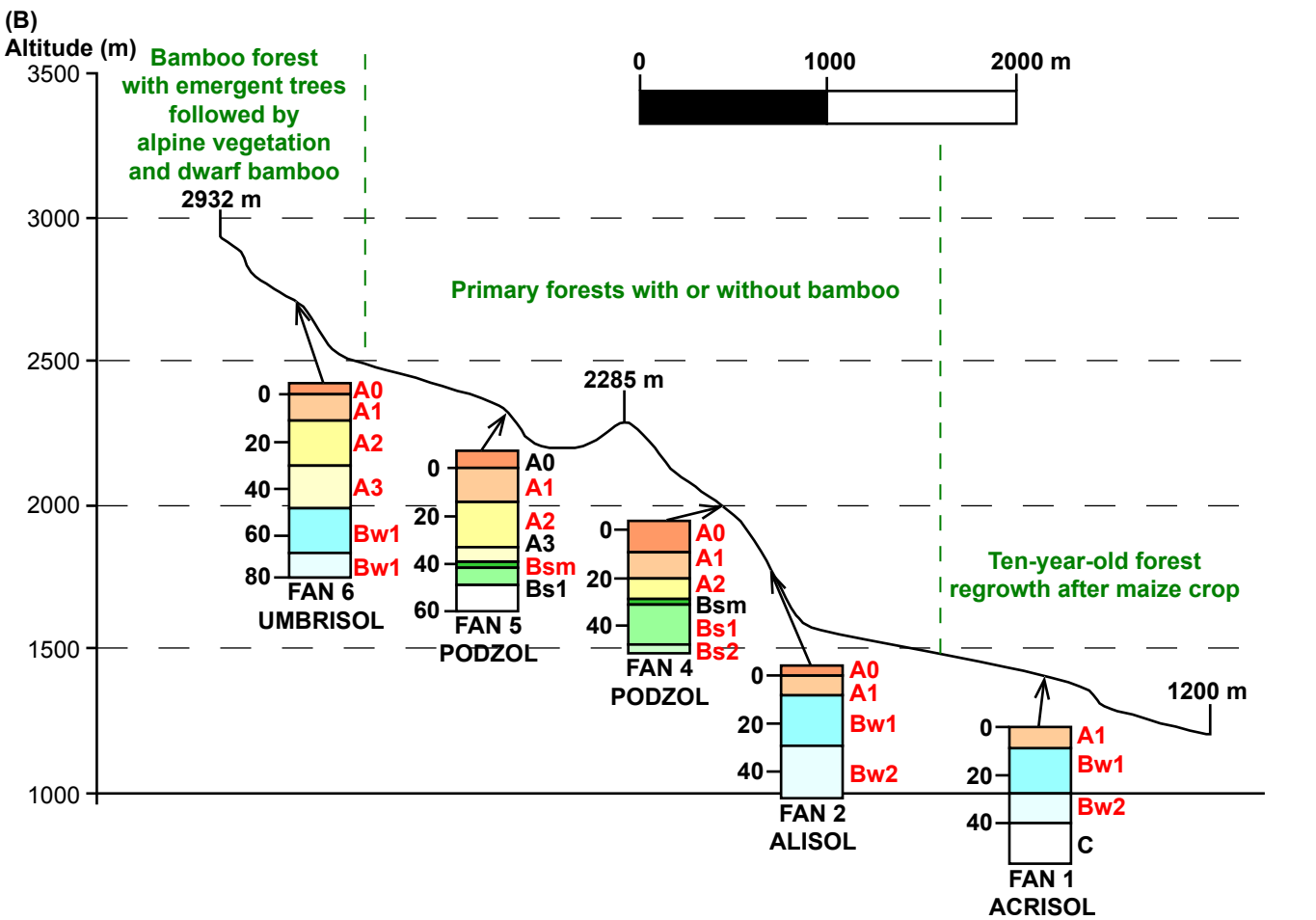

Figure 3 - revised

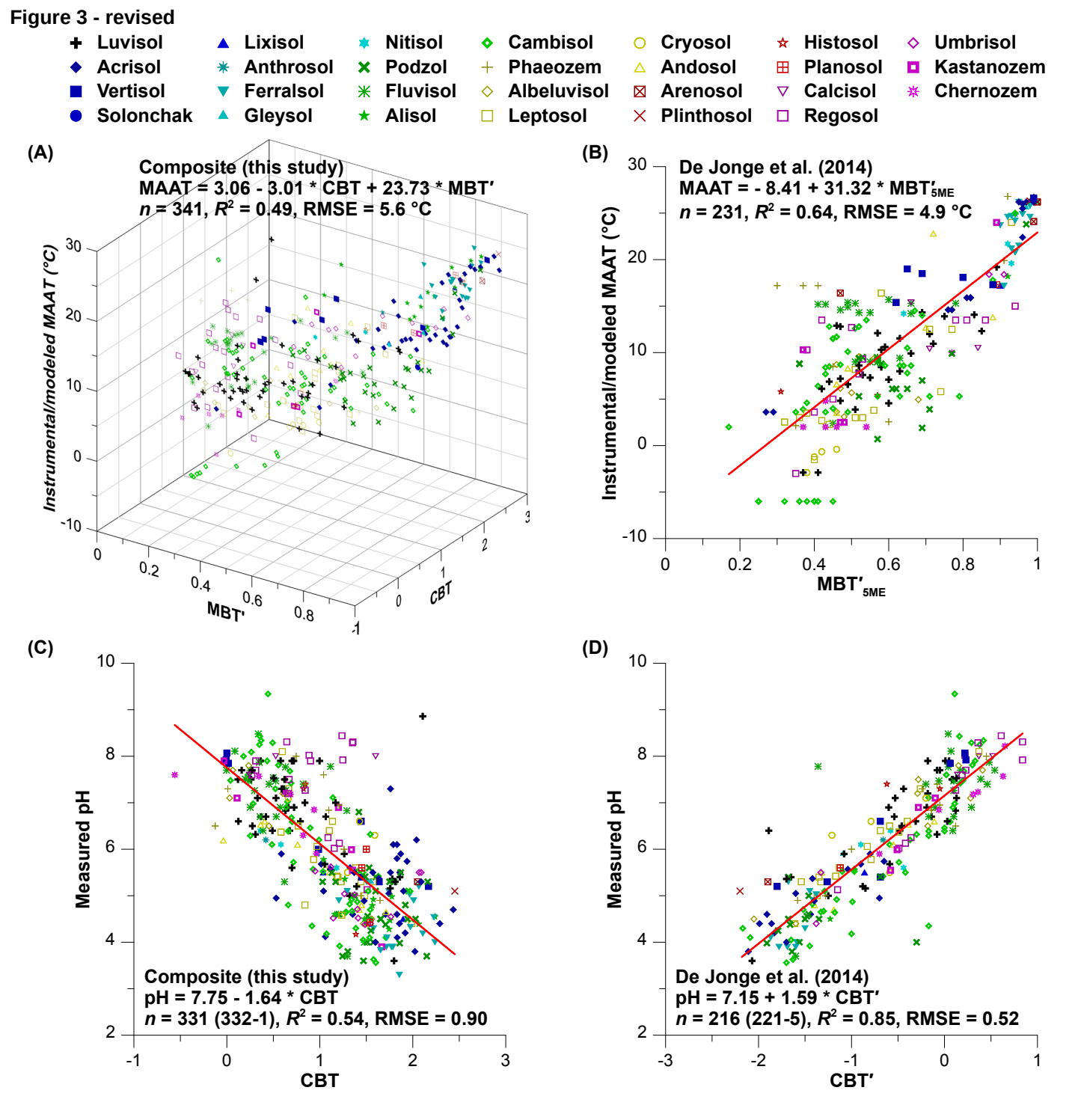

Figure 4 - revised

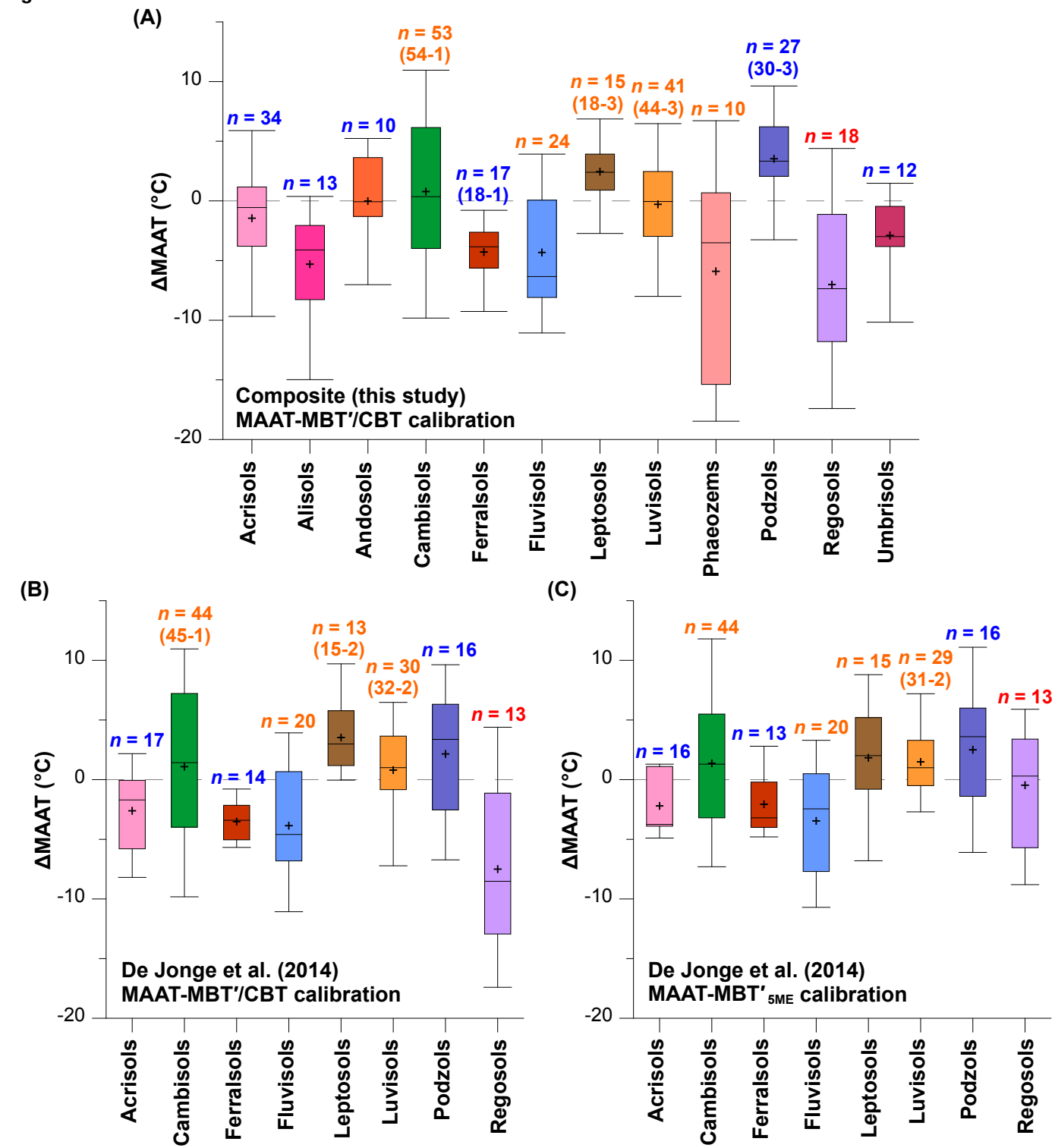

Figure 5 - revised

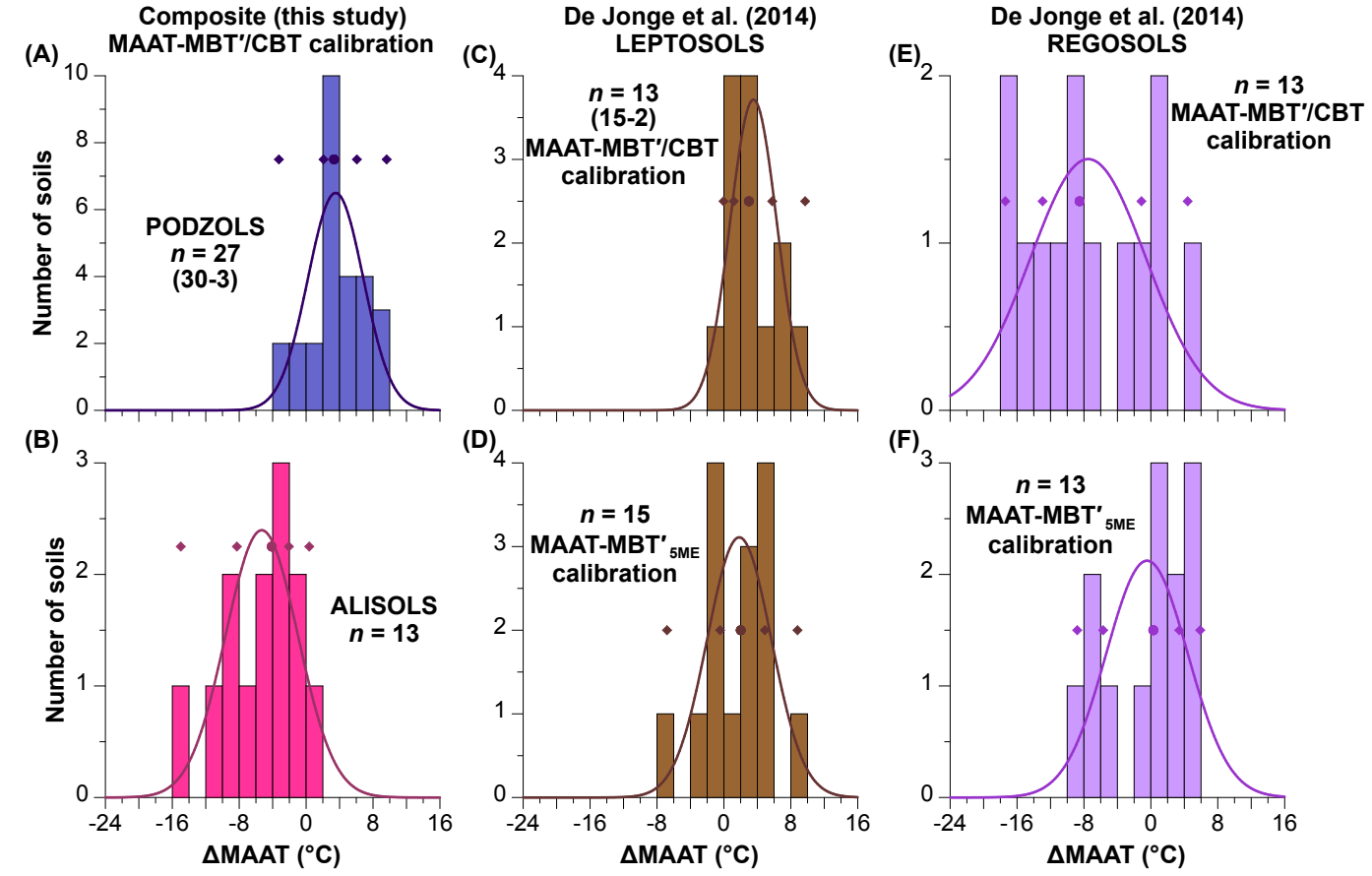

Figure 6

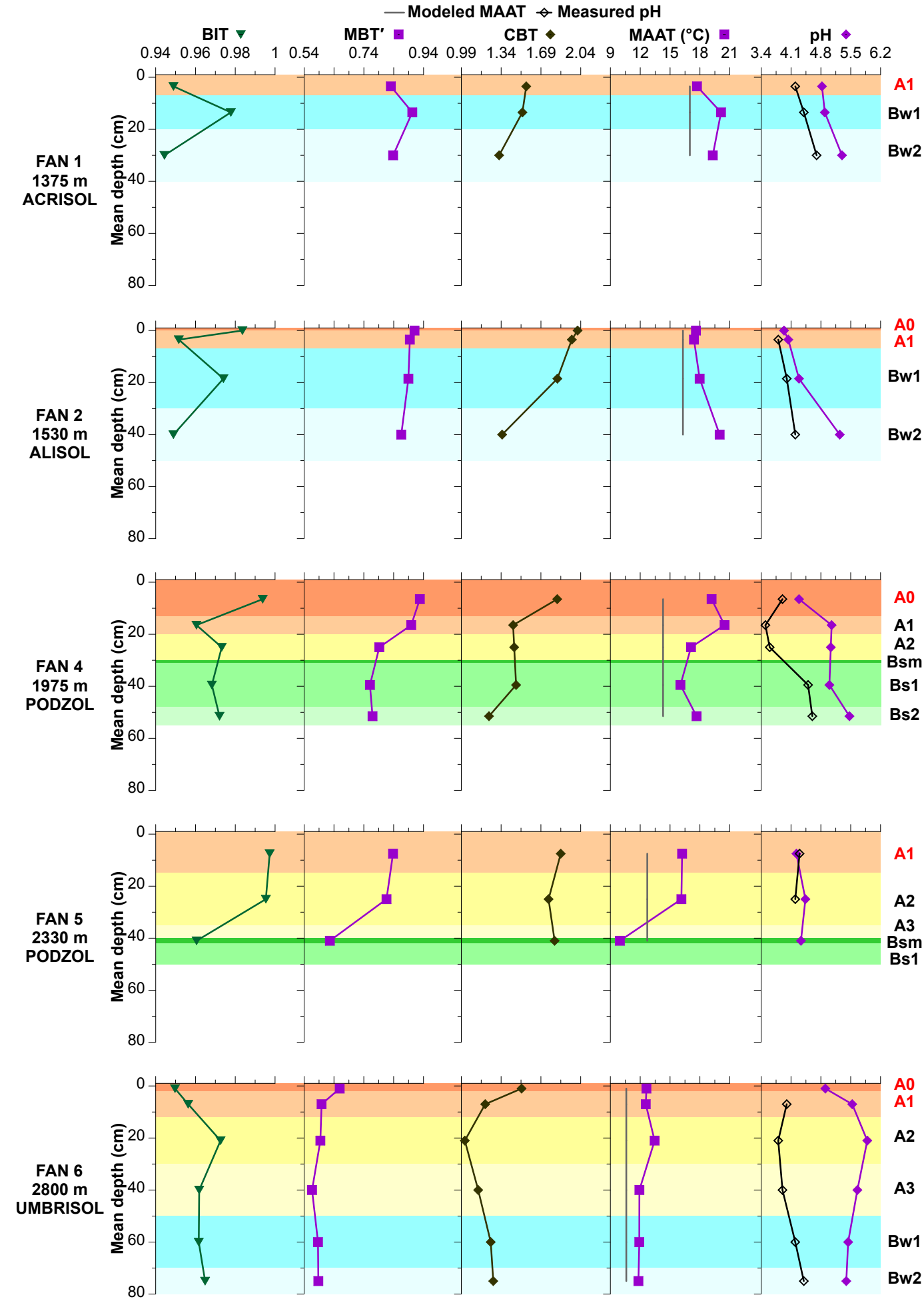
Modeled MAAT
Measured pH
BIT
MBT′
CBT
MAAT (°C)
pH
0.94 0.96 0.98 1
0.54 0.74 0.94
0.99 1.34 1.69 2.04
9 12 15 18 21
3.4 4.1 4.8 5.5 6.2
Mean depth (cm)
0 20 40 60 80
FAN 1
1375 m
ACRISOL
A1
Bw1
Bw2
FAN 2
1530 m
ALISOL
A0
A1
Bw1
Bw2
FAN 4
1975 m
PODZOL
A0
A1
A2
Bsm
Bs1
Bs2
FAN 5
2330 m
PODZOL
A1
A2
A3
Bsm
Bs1
FAN 6
2800 m
UMBRISOL
A0
A1
A2
A3
Bw1
Bw2

Table 1

	MAAT = a * MBT′ + b * CBT + c						pH = S * CBT + I					
	n	a	b	c	R^2	*p*	E	*n*	S	I	R^2	*p*	E
All soils	341	23.73 ± 1.43	–3.01 ± 0.65	3.06 ± 0.72	0.5	< 0.001	5.6	331 (332–1)	–1.64 ± 0.08	7.75 ± 0.11	0.5	< 0.001	0.9
Acrisols	33 (34–1)	38.23 ± 3.71	–4.20 ± 1.48	–6.32 ± 2.72	0.8	< 0.001	3.1	33	–0.16 ± 0.32	5.45 ± 0.53	0.0	0.61	0.8
Alisols	13	0.46 ± 5.49	4.49 ± 2.17	15.37 ± 4.17	0.4	0.10	2.3	13	–0.66 ± 0.30	5.79 ± 0.49	0.3	0.052	0.4
Andosols	10	24.61 ± 9.77	–4.22 ± 2.61	2.89 ± 6.10	0.6	0.049	4.4	10	–1.28 ± 0.23	6.74 ± 0.25	0.8	< 0.001	0.4
Cambisols	54	23.64 ± 5.27	–7.20 ± 1.91	4.72 ± 2.18	0.3	< 0.001	6.3	53	–2.32 ± 0.25	8.25 ± 0.27	0.6	< 0.001	0.9
Ferralsols	18	24.07 ± 15.22	–1.90 ± 2.12	5.05 ± 14.80	0.2	0.21	2.5	18	–0.42 ± 0.50	5.19 ± 0.91	0.0	0.41	0.6
Fluvisols	24	5.16 ± 7.84	–0.66 ± 2.72	11.45 ± 2.23	0.0	0.78	3.8	24	–1.91 ± 0.49	8.06 ± 0.33	0.4	0.001	0.9
Leptosols	18	30.55 ± 6.70	–2.19 ± 3.34	–4.63 ± 3.95	0.6	0.001	4.6	18	–1.89 ± 0.44	7.92 ± 0.53	0.5	0.001	0.7
Luvisols	42 (44–2)	15.02 ± 2.78	–4.09 ± 1.02	5.83 ± 1.21	0.5	< 0.001	3.1	40 (41–1)	–1.46 ± 0.22	7.81 ± 0.20	0.5	< 0.001	0.7
Phaeozems	10	4.79 ± 8.88	–7.19 ± 4.19	18.33 ± 6.17	0.4	0.21	7.0	10	–0.95 ± 0.55	7.52 ± 0.59	0.3	0.12	1.0
Podzols	30	23.24 ± 5.53	–2.48 ± 2.98	–1.74 ± 4.75	0.4	0.001	4.3	29	–0.32 ± 0.48	5.27 ± 0.77	0.0	0.51	0.8
Regosols	17 (18–1)	–8.65 ± 8.55	4.27 ± 2.12	7.69 ± 2.35	0.2	0.15	3.4	17	–0.73 ± 0.60	8.07 ± 0.60	0.1	0.25	1.0
Umbrisols	12	15.34 ± 3.92	–0.89 ± 2.15	6.71 ± 3.05	0.7	0.01	2.2	12	0.09 ± 0.43	4.81 ± 0.65	0.0	0.84	0.5

Table 2

		All soils	Acrisols	Cambisols	Ferralsols	Fluvisols	Leptosols	Luvisols	Podzols	Regosols
MAAT = a × MBT′ + b × CBT + c	*n*	234 (235–1)	17	45	14	19 (20–1)	15	30 (32–2)	16	12 (13–1)
	a	27.47 ± 1.79	37.02 ± 2.99	23.61 ± 6.27	37.78 ± 14.23	–10.47 ± 9.61	28.52 ± 8.02	22.14 ± 4.70	24.32 ± 9.20	–22.85 ± 9.57
	b	–4.53 ± 0.78	–2.53 ± 1.23	–7.05 ± 2.29	–3.92 ± 1.69	1.33 ± 2.94	–1.84 ± 3.87	–5.28 ± 1.16	–3.05 ± 6.42	3.81 ± 2.24
	c	2.35 ± 0.88	–6.48 ± 2.33	4.28 ± 2.66	–4.99 ± 14.52	15.77 ± 2.37	–4.34 ± 4.48	3.42 ± 2.02	–1.43 ± 9.82	12.02 ± 2.96
	R^2	0.5	0.9	0.3	0.6	0.1	0.5	0.6	0.4	0.5
	p	< 0.001	< 0.001	0.001	0.003	0.44	0.01	< 0.001	0.053	0.07
	E	5.8	2.3	6.8	1.6	2.9	5.0	3.2	5.9	3.0
MAAT = S × MBT'_{5ME} + I	*n*	231	16	44	13	20	15	31	16	13
Homogeneity of slopes test:	S	31.32 ± 1.55	32.96 ± 2.79	31.21 ± 5.31	50.07 ± 28.84	3.91 ± 9.70	31.51 ± 6.27	25.80 ± 4.40	24.41 ± 7.99	15.98 ± 5.75
$F = 1.59$, $p = 0.14$	I	–8.41 ± 1.01	–7.65 ± 2.40	–9.74 ± 2.80	–24.01 ± 27.14	10.17 ± 5.39	–10.36 ± 3.57	–6.18 ± 2.62	–6.59 ± 5.25	0.61 ± 3.43
ANCOVA:	R^2	0.6	0.9	0.5	0.2	0.0	0.7	0.5	0.4	0.4
$F = 5.34$, $p < 0.001$	*p*	< 0.001	< 0.001	< 0.001	0.11	0.69	< 0.001	< 0.001	0.01	0.02
	E	4.9	2.5	5.6	2.4	3.7	4.1	3.2	5.5	4.1
pH = S × CBT + I	*n*	231 (232–1)	16	44	14	20	15	31 (32–1)	16	13
Homogeneity of slopes test:	S	–1.75 ± 0.10	–0.63 ± 0.27	–2.44 ± 0.29	–0.56 ± 0.63	–2.20 ± 0.51	–2.11 ± 0.36	–1.55 ± 0.23	–0.54 ± 0.50	–0.77 ± 0.80
$F = 3.83$, $p = 0.001$	I	7.90 ± 0.12	5.86 ± 0.44	8.35 ± 0.31	5.47 ± 1.12	8.18 ± 0.32	8.31 ± 0.42	7.84 ± 0.22	5.32 ± 0.83	8.11 ± 0.86
	R^2	0.6	0.3	0.6	0.1	0.5	0.7	0.6	0.1	0.1
	p	< 0.001	0.03	< 0.001	0.39	< 0.001	< 0.001	< 0.001	0.30	0.36
	E	0.9	0.6	0.9	0.7	0.9	0.5	0.7	0.5	1.1
pH = S × CBT′ + I	*n*	216 (221–5)	15	42 (44–2)	10	17 (19–2)	15	31	14	12
Homogeneity of slopes test:	S	1.59 ± 0.05	1.14 ± 0.20	1.78 ± 0.10	1.97 ± 1.03	0.56 ± 0.61	1.66 ± 0.11	1.29 ± 0.18	0.18 ± 0.33	1.76 ± 0.19
$F = 4.64$, $p < 0.001$	I	7.15 ± 0.05	6.49 ± 0.30	7.04 ± 0.10	7.59 ± 1.65	7.32 ± 0.16	7.43 ± 0.12	7.25 ± 0.14	4.75 ± 0.49	7.11 ± 0.11
	R^2	0.8	0.7	0.9	0.3	0.1	0.9	0.6	0.0	0.9
	p	< 0.001	< 0.001	< 0.001	0.09	0.37	< 0.001	< 0.001	0.59	< 0.001
	E	0.5	0.4	0.5	0.5	0.5	0.2	0.6	0.5	0.4

Table 3

Sample	Altitude (m)	Coordinates	Horizon	Mean depth (cm)	C_{org} (%)	H_2O (%)	Measured pH	Modeled MAAT (°C)	BIT	MBT′	CBT	Calculated MAAT (°C)	Calculated pH
FAN1.1	1375	22°19′15″N 103°49′52″E	A1	3.5	8.27	76	4.2	17.0	0.95	0.83	1.56	17.7	4.8
FAN1.2			Bw1	13.5	2.72	nd	4.4		0.98	0.90	1.53	20.1	4.9
FAN1.3			Bw2	30	0.62	60	4.7		0.94	0.84	1.32	19.3	5.3
FAN2.A0	1530	22°18′44″N 103°49′25″E	A0	0	nd	nd	nd	16.3	0.98	0.91	2.01	17.6	3.9
FAN2.1			A1	3.5	4.30	80	3.8		0.95	0.89	1.96	17.4	4.0
FAN2.2			Bw1	18.5	2.54	nd	4.0		0.97	0.89	1.83	18.0	4.3
FAN2.3			Bw2	40	0.66	50	4.2		0.95	0.87	1.35	20.0	5.2
FAN4.1	1975	22°18′20″N 103°48′38″E	A0	6.5	44.13	nd	3.9	14.3	0.99	0.93	1.83	19.2	4.3
FAN4.2			A1	16.5	8.11	215	3.5		0.96	0.90	1.45	20.5	5.1
FAN4.3			A2	25	3.59	66	3.6		0.97	0.79	1.46	17.1	5.0
FAN4.5			Bs1	39.5	1.22	40	4.5		0.97	0.76	1.47	16.0	5.0
FAN4.6			Bs2	51.5	1.16	nd	4.6		0.97	0.77	1.23	17.7	5.5
FAN5.1	2330	22°18′00″N 103°48′36″E	A1	7.5	5.99	114	4.3	12.7	1.00	0.84	1.86	16.2	4.2
FAN5.2			A2	25	4.38	nd	4.2		1.00	0.82	1.76	16.1	4.4
FAN5.4			Bsm	41	nd	nd	nd		0.96	0.63	1.81	10.0	4.3
FAN6.1	2800	22°17′32″N 103°48′02″E	A0	1	6.14	nd	nd	10.6	0.95	0.66	1.52	12.6	4.9
FAN6.2			A1	7	3.89	106	4.0		0.96	0.60	1.20	12.6	5.5
FAN6.3			A2	21	2.95	nd	3.8		0.97	0.59	1.02	13.5	5.9
FAN6.4			A3	40	2.07	53	3.9		0.96	0.57	1.14	11.9	5.7
FAN6.5			Bw1	60	0.77	nd	4.2		0.96	0.59	1.25	11.9	5.4
FAN6.6			Bw2	75	0.39	nd	4.4		0.96	0.59	1.27	11.8	5.4